Desalination and Water Treatment
www.deswater.com

doi: 10.5004/dwt.2022.28550

260 (2022) 299–308
June

Elaboration of innovative ceramic microfiltration membrane from natural Moroccan sand for wastewater treatment

Mourad Addich[a,*], Noureddine El Baraka[a], Nabil Saffaj[b], Abdellatif Laknifli[a], Abdelaali Karim[c], Karim Sbihi[a], Abdellatif El Hammadi[a]

[a]*Laboratory of Biotechnology, Materials, and Environment, Research-Research Team, Physicochemistry of Natural Environments, Materials, and Environment, University Ibn Zohr, Polydisciplinary Faculty of Taroudant, Morocco, emails: mourad.addich@gmail.com (M. Addich), n.elbaraka@uiz.ac.ma (N. El Baraka), a.laknifli@uiz.ac.ma (A. Laknifli), sbihikarim7@gmail.com (K. Sbihi), a.elhammadi@uiz.ac.ma (A. El Hammadi)*
[b]*Laboratory of Biotechnology, Materials, and Environment, Research-Research Team, Natural Substances & Environment, University Ibn Zohr, Polydisciplinary Faculty of Ouarzazat, Morocco, email: saffaj@gmail.com*
[c]*Laboratory of Materials, Membranes and Environment, Faculty of Sciences and Techniques Mohammedia, Hassan II University of Casablanca, email: karimabdelaali@gmail.com*

Received 10 December 2021; Accepted 1 May 2022

ABSTRACT

This paper aims to elaborate a ceramic membrane made of natural Moroccan sand. The raw material was characterized using X-ray diffraction, energy-dispersive X-ray spectroscopy, thermogravimetric analysis and Fourier-transform infrared spectroscopy techniques. Sand powder (average particle size = 100 μm) was mixed with organic additives and water to produce a plastic paste with rheological properties that allowed for extrusion shaping. Heat treatment of flat membrane support with a diameter of 4 cm and a thickness of 2 mm at 1,050°C/2 h resulted in porosity of 44.04%. The active microfiltration layer was prepared from the same natural sand powder (average particle size < 50 μm) by the spin coating method from 8 wt.% of sand powder 62 wt.% of water and 30 wt.% of PVA (polyvinyl alcohol). The scanning electron microscope was used to examine the formed membrane. The experimental results indicate that sand membrane efficiently clarifies citrus wash effluent. It was shown that chemical oxygen demand and turbidity removals could achieve 64% and 99.8%, respectively.

Keywords: Ceramic support; Membrane; Microfiltration; Sand; Water treatment

1. Introduction

Water pollution is one of the most pressing challenges in the world, and it is mainly caused by the world's growing population and industrialization. Water pollution has a negative impact on both human health and the environment; therefore, water treatment technologies have been developed with considerable care. One of the promising water treatment technologies presently advanced is membrane technology, that's taken into consideration a promising technique because of its easy operation. Nowadays, due to their simple functionality and high porosity, polymer-based membranes are readily available. Furthermore, polymeric membranes do not endure long in hostile conditions, such as high temperatures and corrosive chemicals. As a result, there are concerns regarding their long-term

* Corresponding author.

Presented at the 9th International Conference on Water Resources in the Mediterranean Basin (WATMED9), 26–28 May 2021, Marrakech, Morocco

usability, prompting additional efforts to produce more durable membranes, such as ceramic membranes that can withstand harsh conditions and last longer [1].

Ceramic membranes possess several desirable mechanical and chemical properties such as resistance to corrosive environments, high thermal stability, mechanical strength and relative inertness [2]. Membrane technologies are commonly used in various disciplines, including chemistry, biotechnology, food, and, more recently, wastewater treatment [3,4]. Due to the high flow of microfiltration compared to other membrane processes, microfiltration (MF) is the membrane process that could treat maximum liquid volume under low transmembrane pressure when compared to a nanofiltration (NF) and reverse osmosis (RO) [5]. In addition, microfiltration separation is based on a sieving mechanism which makes microfiltration membrane relatively more suitable for most industrial wastewater. The selection of an adequate membrane depends on several parameters that should be taken into consideration, such as targeted species, amount of wastewater and operating conditions.

Ceramic membranes are often made up of many layers that form an asymmetric structure and are manufactured from titania (TiO_2), silica (SiO_2), alumina (Al_2O_3), and zirconia (ZrO_2) [1,5]. These raw materials are expensive and necessitate high sintering temperatures (1,300–1,500°C) [6,7]. Therefore, to make ceramic membranes economically viable, raw material costs and sintering temperatures should be reduced to a minimum. Furthermore, inorganic membranes are often quoted as being at least ten times more expensive than polymeric membranes, with a cost range of 500–3,000 $/m^2 [7]. However, there is a lot of scope to make ceramic membranes with low-cost raw materials and preserve their advantages. Furthermore, utilizing low-cost ceramic materials, sintering temperatures can be decreased, that is, below 1,500°C. To substitute pricey raw materials, various alternatives have been developed, including silica, alumina, zirconia, and titania. Ceramic membranes have been made using naturally occurring clays such as kaolin clay [8], bentonite clay [9], and dolomite [10], as well as other earth minerals such as natural pozzolan [11,12], magnesite [13,14], phosphate [3,15], and perlite [16].

The sand is used to neutralize acidic components and reach the desired pH levels in water filtering. The material also has absorbent qualities, which help remove granular pollutants, suspended particles, and colloids from water. As a result, silica sand has a range of features in water filtration [17], including strong durability and acidic chemical resistance, all of which contribute to its mechanical strength. In membrane manufacturing, there are a variety of desirable properties.

The aim of the research is to develop a novel low-cost membrane for MF of citrus wash effluent produced from Moroccan natural sand. X-ray fluorescence (XRF), X-ray diffraction (XRD), Fourier-transform infrared spectroscopy (FTIR), and thermogravimetric analysis (TGA) were used to analyze raw sand. Dry uniaxial pressing and sintering were used to manufacture the ceramic membrane. The influence of sintering temperature on the membrane's physical, mechanical, and morphological properties was also examined. Finally, the improved membrane was used to treat MF of citrus wash effluent, particularly that produced by a local citrus cooperative.

2. Materials and methods

2.1. Sand powder

In this study, natural sand was selected as the starting material for fabrication of ceramic MF membrane. The city of Agadir was the source of the raw sand. The distribution of the various dimensions of raw sand is shown in Fig. 1:

This powder is characterized by XRD, FTIR spectroscopy and TGA, differential thermal analysis (DTA). Scanning electron microscopy with energy-dispersive X-ray spectrometry (SEM/EDX) was used to determine the chemical composition (weight percent) of this powder.

2.2. Preparation of porous support

Three steps are required in the preparation of membrane support:

- Crushing and sieving at 100 μm the powder;
- Formulating a plastic paste;
- Extrusion;
- Sintering to consolidate.

Fig. 2 shows ceramic support preparation process. A paste with rheological properties is created with a mixture of plasticizer and binder and sand powder, organic additives, and water. The main benefit of these additives is that they are burned away during the sintering process. The paste is obtained by mixing:

- Sand powder 82 wt.%;
- Amidon 10 wt.%;
- Amijel 4 wt.%;
- Methocel 4 wt.%;
- Adding the water (28.4 wt.% of powders) and glycerin 0.5 wt.%.

After 2 d of high humidity, the paste has fully diffused the water and organic additives, preventing premature

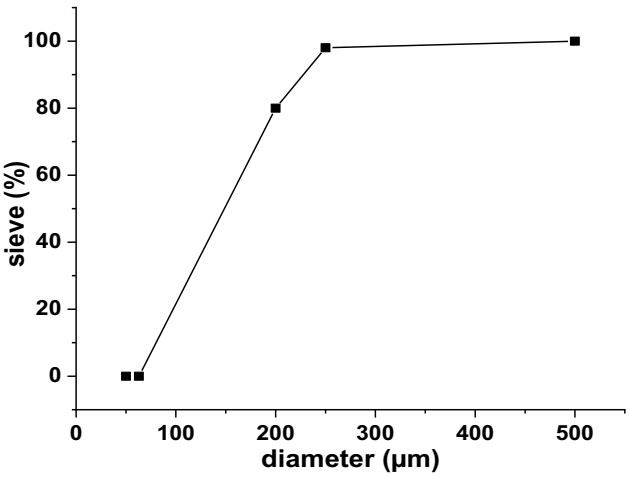

Fig. 1. Grain size distribution of sand studied.

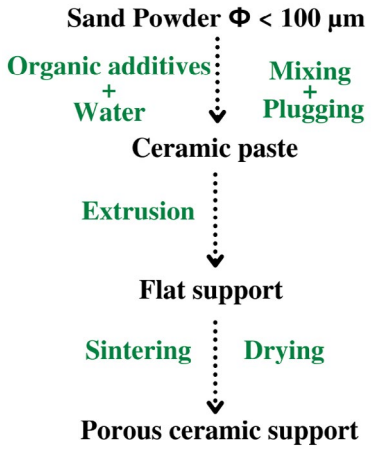

Fig. 2. Main steps of the ceramic support preparation.

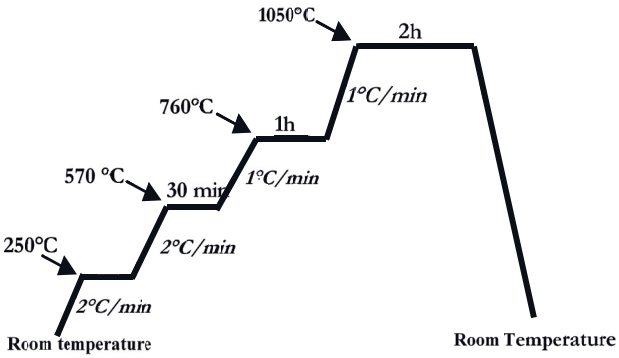

Fig. 3. Thermal treatment of sintering the flat support.

drying. Extrusion was used to shape the material, which was then calendared into a thin film segmented to form flat disk supports with a diameter of 4 cm. The wet support was scheduled to have a uniform drying at 40°C for 24 h after extrusion. Finally, sintering at various final temperatures has been permitted in a programmable furnace. The choices of different plateaus are based on the DTA/TGA analysis, this is to give each transformation the necessary duration. The sintered fragments were extruded at a temperature of 1,000°C, 1,050°C and 1,100°C (Fig. 3).

2.3. Preparation of the microfiltration layer

A slip casting method was made by combining 8 wt.% of the same natural powder (≤50 µm), 62 wt.% water, and 30 wt.% polyvinyl alcohols (12% w/w aqueous solution). The sand support was coated using clay suspension by spin-coating method (Fig. 4). Then, the green membrane was dried at room temperature for overnight. Thereafter, the membrane was heated at temperature of 250°C for 2 h to completely eliminate PVA (polyvinyl alcohol). Subsequently, it was sintered at 1,050°C for 2 h.

2.4. Characterization techniques

The support and membrane prepared was observed by SEM (JEOL JSM IT-100 Type, Japan). When using membranes, a cleaning cycle is needed to regenerate. In most cases, industrial mineral membranes are regenerated using a protocol that alternates with basic and acid solutions. Chemical attack tests were carried out every 24 h for 150 h at room temperature (25°C) in acid (HCl; 0.1 N) and basic (NaOH; 0.1 N) solutions. We calculated the percentage of mass loss after washing and drying. Moreover, the mechanical resistance tests were carried out using the three-point bending method (Shimadzu EZ-LX, Japan). ASTM C373-88 standard is followed for porosity tests of support.

2.5. Filtration test

Filtration experiments were conducted on a laboratory scale using the fontal filtration pilot (Fig. 5). The filtration on the membrane is visualized using a clear pyrex glass filtration cell in this pilot. Variation of the feed height H controls the pressure of the fluid exerted on the membrane, which is given by the equation $\Delta P = \rho \cdot g \cdot \Delta h$ (ρ: volumic mass; h: feeding height from the ground; g: gravity). The hydraulic permeability (L_p) can be determined using the variation of the distilled water flux (J_w) with the trans membrane pressure ΔP (bar) by following the Darcy's law [Eq. (1)].

$$F = L_p \cdot \Delta P \tag{1}$$

At first, the water permeability of a support with a filtration area of 15.20 cm^2 and a thickness of 2 mm was measured. Before filtration a test, the support was submerged in ultrapure water for at least 24 h.

The flux was measured at different pressures (0.01, 0.02, 0.03, and 0.04 bar) and the permeability was calculated from the flux of each pressure. The permeate was collected and characterized systematically every 20 min during filtration time of 2 h at constant transmembrane pressure of 0.04 bar. Every 20 min, physico-chemical parameters of the permeate, including pH, turbidity, chemical oxygen demand (COD) and conductivity, were tested to assess the membrane's separation performance. The rejection R (%) was given by Eq. (2):

$$R(\%) = \frac{X_{\text{feed}} - X_{\text{permeate}}}{X_{\text{feed}}} \times 100x \tag{2}$$

where X_{feed} and X_{permeate} are physico-chemical parameters of the feed and the permeate respectively.

3. Results and discussion

3.1. Characterization of the sand powder

3.1.1. Chemical composition

Chemical composition of natural sand is reported in Table 1. It can be clearly seen that sand is mainly composed of SiO_2, $CaCO_3$ and Al_2O_3. These oxides are generally presented in natural sand in the form of quartz, calcite, dolomite and albite as seen in the XRD pattern (Fig. 7).

Energy-dispersive X-ray spectroscopy analysis (Fig. 6) has shown that sand consists of quartz, alumina, calcite and aragonite, following the previous result.

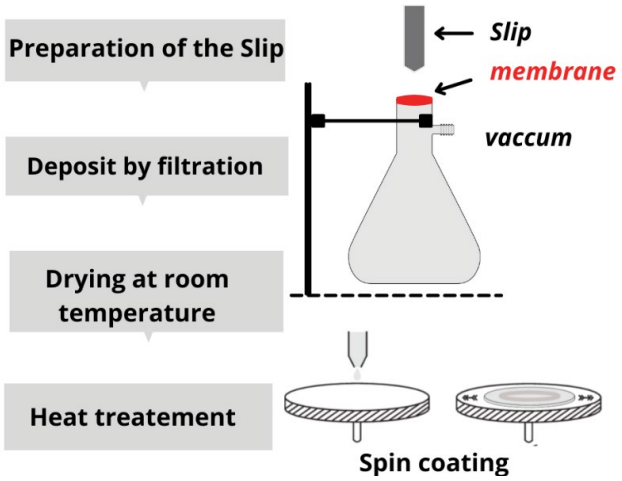

Fig. 4. Preparation of the microfiltration layer.

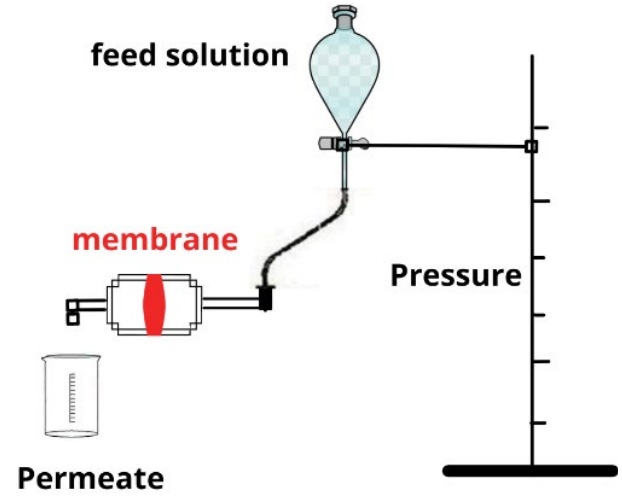

Fig. 5. Frontal filtration pilot.

3.1.2. FTIR analysis

Fig. 8 presents the FTIR spectra of sand powder. From the figure, sand powder exhibited a band at 3,520 cm^{-1} representing the hydroxyl group [2]. The patterns of CO_2 were shown around 2,340–2,360 cm^{-1} [18]. While the symmetric stretching vibration of the carbonate group is related to the band at 1,460 cm^{-1} [13]. With $A \simeq 1$, the spectrum was saturated around 1,000–1,002 cm^{-1} (Si–O stretch) generally due to a silicate structure [19,20]. Meanwhile, the small band around 470 and 800 cm^{-1} is due to the presence of quartz phase [21,22]. The sharp band at 470–520 cm^{-1} is sometimes observed and depends on the internal structure of the amorphous silica [23].

3.1.3. Thermogravimetric analysis

Thermal study aims to identify temperature regimes in the membrane where the majority of weight losses and consequently changes actually occur. TGA and DTA of the powder mixture when subjected to thermogravimetric analysis by heating the dry inorganic mixture in alumina crucible from room temperature to 1,000°C at a heating rate of 10°C/min, as shown in Fig. 9.

Two endothermic peaks were discovered. The first peak appears at 100°C with weight loss of 0.5 wt.% is due to elimination of free and absorbed water [24]. The second peak appears between 700°C and 800°C with weight loss of 6 wt.% as result from decomposition of carbonates and

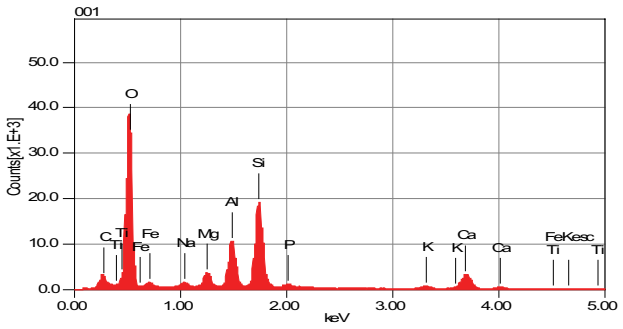

Fig. 6. Energy-dispersive X-ray spectroscopy of sand.

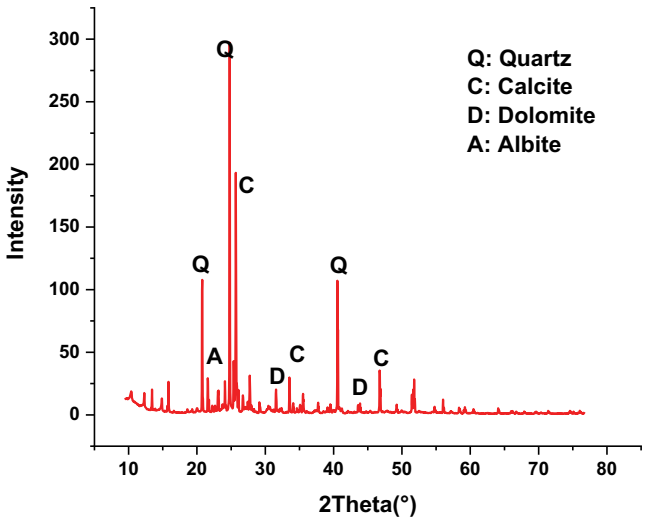

Fig. 7. X-ray diffractogram of sand powder.

Table 1
Chemical composition (wt.%) of sand powder

Components of sand	Weight percent (%)
SiO_2	83.13
$CaCO_3$	7.94
Al_2O_3	4.36
CaO	1.53
FeO	0.77
MgO	0.71
P_2O_5	0.52
K_2O	0.20
Na_2O	0.72
TiO_2	0.12

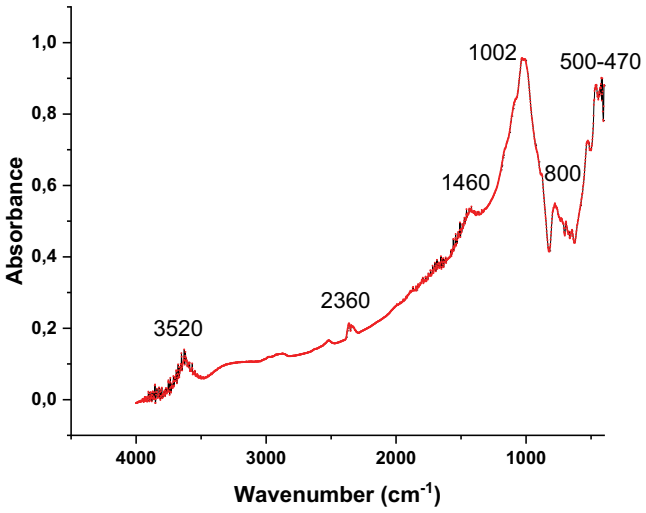

Fig. 8. Infrared spectrum of sand powder.

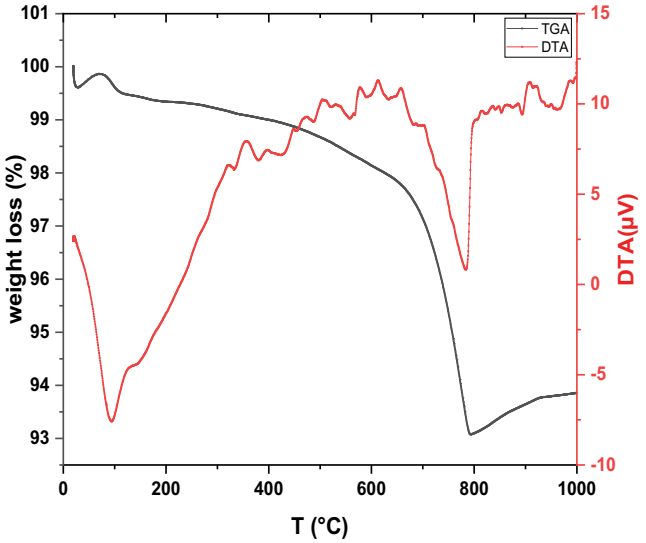

Fig. 9. Thermoanalytical curves of raw sand.

hydroxyls [19]. Another interpretation proposal due to the elimination of water from the inter-lamellar space.

3.2. Characterization of porous support

Three temperatures were used to sinter the extruded support: 1,000°C, 1,050°C, and 1,100°C. The results of an SEM analysis and mechanical testing of supports sintered at various temperatures were used to determine these sintering temperatures. Sintering produces objects out of powder by heating it in a sintering furnace until the particles stick together. After sintering at 1,100°C, the diameter of the elaborated flat support decreases from 4.2 to 4 cm (Fig. 10); this is due to shrinkage after sintering.

SEM micrographs of top-view sand membrane sintered at temperatures ranging from 1,000°C to 1,100°C are shown in Fig. 11. As can be observed, sintering temperature has a substantial impact on membrane microstructure.

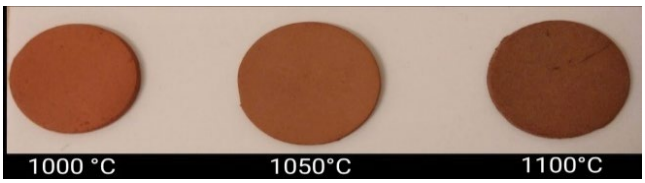

Fig. 10. Images of obtained ceramic membrane sintered at 1,000°C, 1,050°C and 1,100°C.

The sintering has already begun when the sintering temperature is raised to 1,000°C, and small fragments are agglomerated. When the temperature is elevated to 1,050°C, the support surface forms necks between grains, resulting in a robust ceramic body that can withstand hydraulic pressure during filtering tests. Furthermore, the glass phase is dominated due to the vitrification phenomena when the temperature is raised to 1,100°C. As a result of the SEM analysis, it was determined that 1,050°C is the appropriate sintering temperature for manufacturing membrane supports from natural sand.

On the other hand, the area average pore diameter (100 pores) of the support is measured by image processing of SEM pictures using ImageJ. Fig. 7 shows the pore size distribution, which summarizes the calculated percentage pore numbers for various pore diameters. The average pore diameter (d_s) of the support obtained from SEM analysis is determined as follows:

$$d_s = \sqrt{\frac{\sum_{i=1}^{n} n_i d_i^2}{\sum_{i=1}^{n} n_i}} \quad (3)$$

where n is the number of pores, d_i is the pore diameter (µm) of ith pore. The average pore diameters of supports sintered at 1,000°C and 1,050°C are determined as 15.81 and 5.7 µm, respectively (Fig. 12). When sintering temperature was increased to 1,050°C, it is observed that the maximum number of pores (66%–85%) are in the range of 4–6 µm. This morphology is suitable for developing a membrane layer with average pore <1 µm.

3.3. Chemical resistance

Fig. 13 demonstrate that the sand support sintered at 1,050°C has chemical resistance to acid (HCl; 0.1 N) and basic solutions (NaOH; 0.1 N). Weight loss was low when a sample was placed in an aqueous soda solution for 150 h and did not exceed 2% when it was placed in a chloride acid aqueous solution. In terms of color alteration, oxidation, and ageing, no phenomenon has been found after chemical resistance studies.

3.4. Mechanical resistance

Fig. 14 shows the evolution of flexural strength and porosity of sand support prepared at different sintering temperatures. The mechanical strength of the material improves from 13.7 to 17.01 MPa when sintering temperature rises

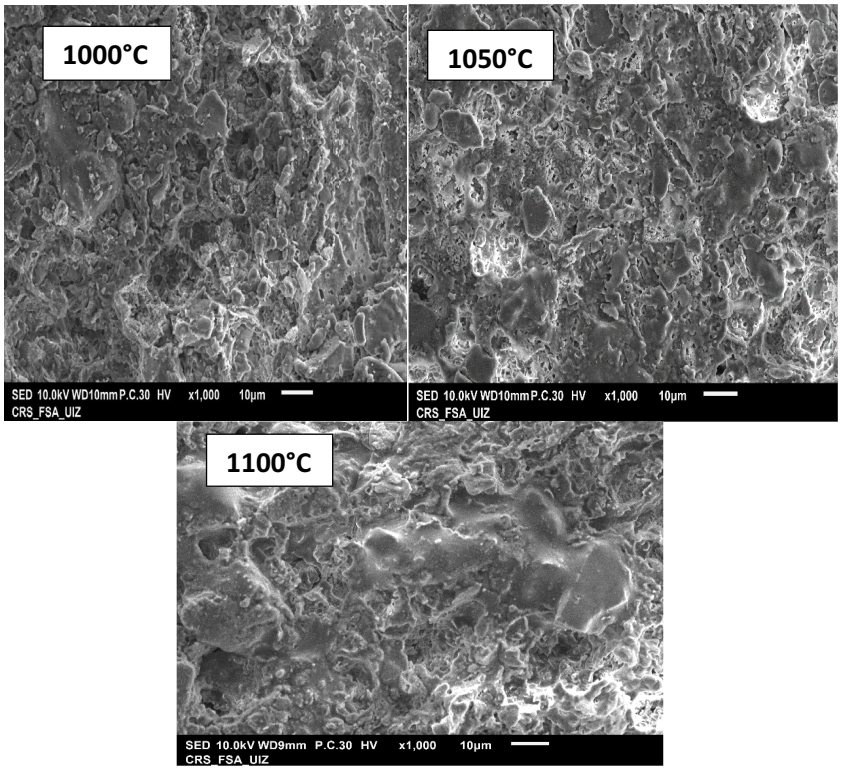

Fig. 11. SEM of supports sintered at different temperatures.

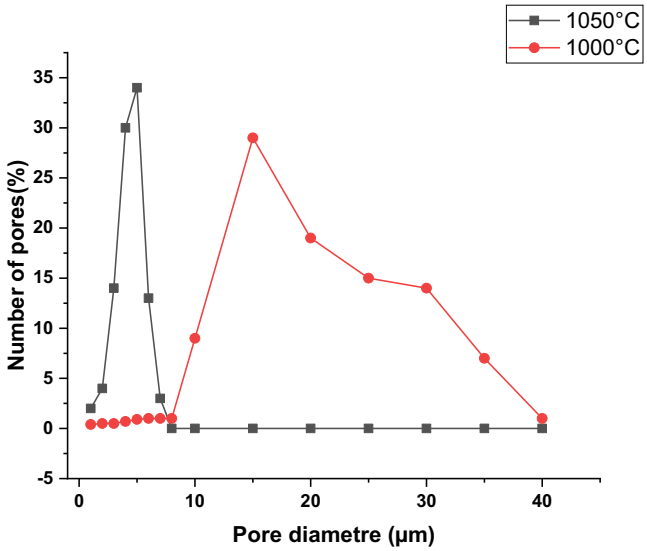

Fig. 12. Pore size distribution of the prepared supports sintered at 900°C and 950°C.

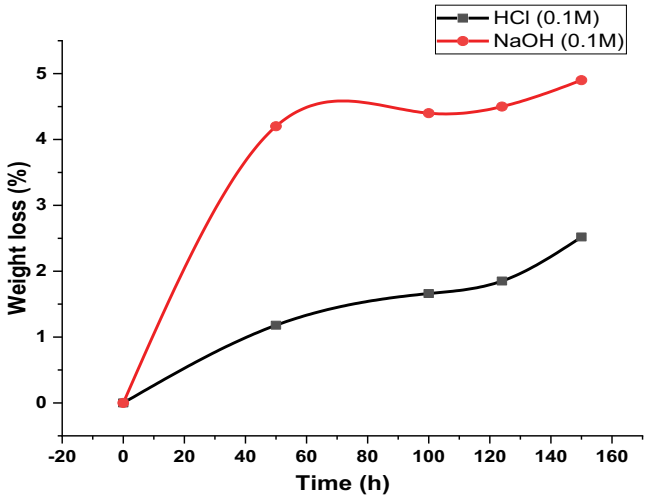

Fig. 13. Chemical resistance.

from 1,000°C to 1,100°C. This is due to the fact that as the sintering temperature rises, the porous structure densifies, allowing for increased structural density while decreasing membrane porosity. Such effects are related to temperature's considerable influence on melt formation, as a result, on the sintering process [25]. Support sintered at 1,000°C has decreased mechanical strength due to absence of boundaries among particles. However, supports sintered at 1,100°C have exciting mechanical strength. But we've got passed the sintering temperature with much less porosity. The sintering temperature is consequently 1,050°C.

3.5. Characterization of the microfiltration layer

SEM was used to examine the morphology and surface quality of the microfiltration layer sintered at 1,050°C/2 h. Fig. 15 display SEM micrographs of the surface and cross section of the microfiltration membrane sintered at 1,050°C/2 h. There are no visible cracks; the support

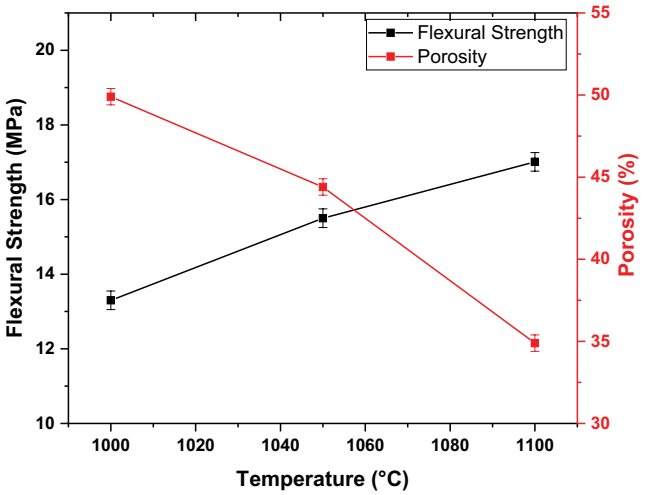

Fig. 14. Flexural strength and porosity.

and microlayer adhere to each other very well. This result supports the good filtration layer deposition conditions observed during the slip casting process. The layer thickness is approximately 84.8 μm. The pore size distribution of the membrane is shown in Fig. 16. Individual pore diameter is measured for about 100 pores using ImgeJ software. The average pore size diameter is about 0.7 μm and 95% of pores have a diameter ≤1.00 μm [Eq. (3)].

3.6. Determination of microfiltration membrane permeability

Water at room temperature was used to test the produced membrane's permeability. Fig. 17 depicts the sand membrane's permeate flux as a function of transmembrane pressure. Two straightly linear curves pass through the origin, as can be shown. As a result of this finding, Darcy's law has been confirmed, and the permeability value can now be calculated using curve slope. Referring to this figure, it shows that permeability decreases from 2,357 to 1,771.4 L/h/m² bar. This drop in permeability could be explained by decrease of porosity because there is a significant connection between porosity and permeability [25].

In the literature studies we find the membrane parameters of the ceramic microfiltration membrane made from different materials as shown in Table 2.

3.7. MF of industrial waste

The optimized sand membrane (sintered at 1,050°C) was used to treat citrus wash effluent generated by a local citrus cooperative as an application to evaluate its performance as an MF membrane. In terms of pH, conductivity,

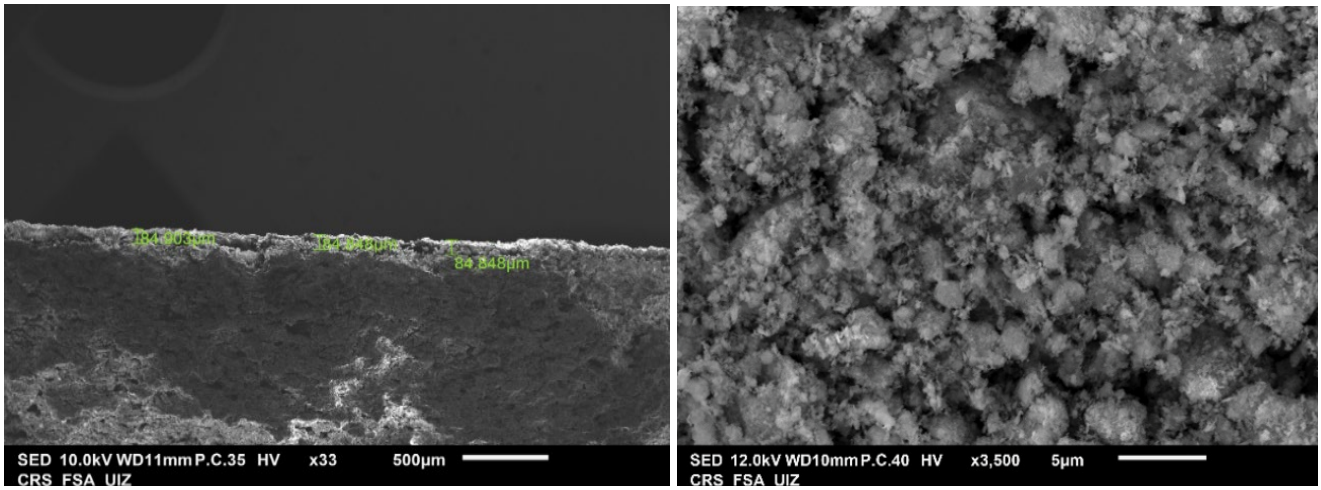

Fig. 15. SEM micrographs of the surface and the cross-section of the microfiltration membrane sintered at 1,050°C.

Table 2
Comparison of manufactured membranes' performance with that of various MF membranes

Materials	Reference	Pore size (μm)	Porosity (%)	Sintering temperature (°C)	Mechanical strength (MPa)	Permeability (L/h/m² bar)
Animal bone	[26]	0.1–1	15.7	1,300	–	1,805
Moroccan clay	[27]	0.19	43	800	–	841
Tunisian natural sand	[28]	1	44.72	1,250	15	1,228
Natural phosphate	[3]	0.26	25.6	1,000	19.7	697
Moroccan sand	This study	0.7	44.04	1,050	15.01	1,771.4

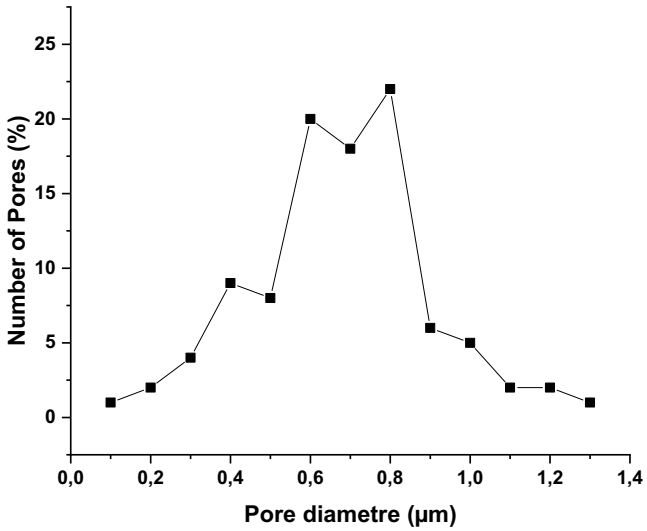

Fig. 16. Pore size distribution of the microfiltration layer prepared.

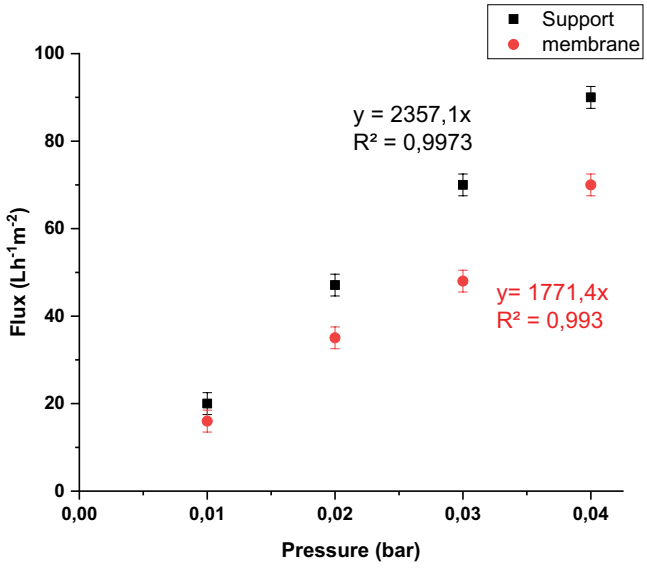

Fig. 17. Water flux permeability of sand support and sand membrane.

COD and turbidity. Table 3 shows the physico-chemical parameters of wastewater. In order to study the performance of produced membranes, these parameters were measured both before and after filtration.

Fig. 18 shows the evolution of permeate flux as a function of filtration time under 0.04 bar pressure for 2 h. As seen in Fig. 20, permeate flux decreases rapidly with filtration time from 53.1–23.7 L/h m^2 due to clogging by particles smaller than membrane pores, which results in internal fouling and the deposition of suspended matter on the membrane surface [14].

Fig. 19 shows the pH of permeate during filtration time and indicates that permeate pH is unchanged over filtration experiment indicating the stability of quality of treated wastewater (cleaning). It should be mentioned

Table 3
Physico-chemical parameters of citrus wash effluent

Parameter	Value
pH	8.10 ± 0.05
Conductivity (mS/cm)	23.7 ± 0.1
COD (mg/L)	785 ± 0.7
Turbidity (NTU)	187 ± 0.6

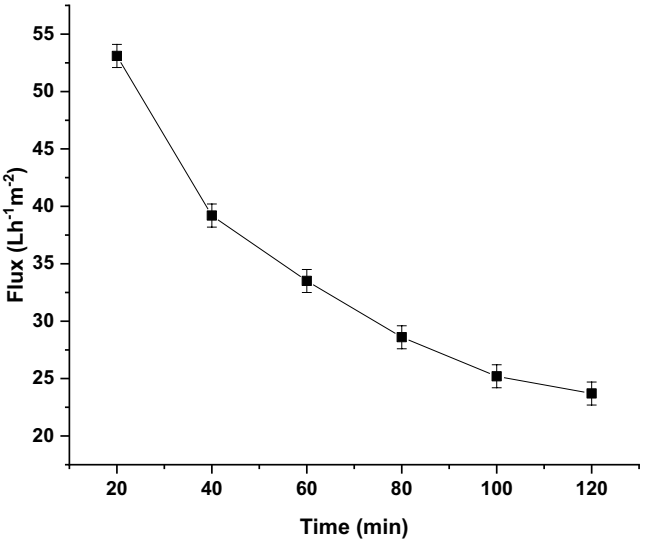

Fig. 18. Permeate flux as a function filtration time.

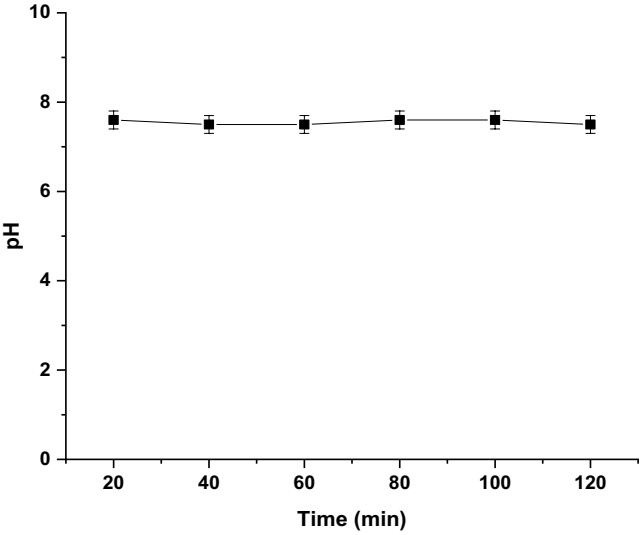

Fig. 19. pH of permeate.

that the pH of wastewater decreases from 8.1 to 7.6 after filtration. The rejection of organic soiling, which is generally characterized by basic features, could be the main cause of the pH drops. Other characteristics, including conductivity, COD, and turbidity, are shown as rejections in Fig. 20 after 2 h of filtration. According to Table 3, the

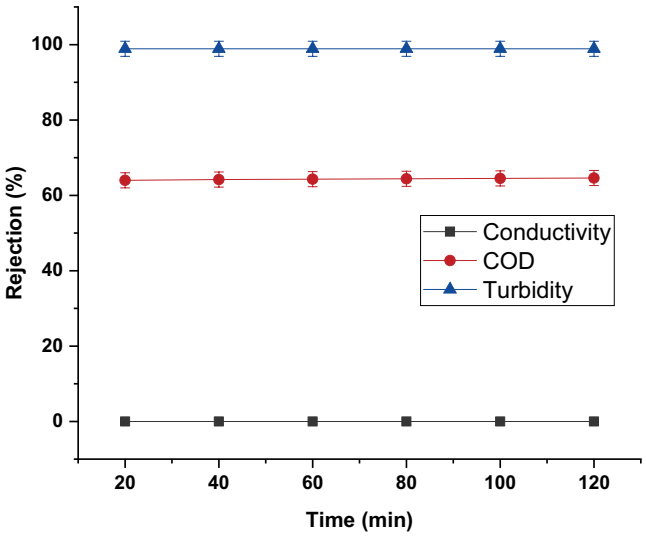

Fig. 20. Turbidity, COD and conductivity rejections of citrus wash effluent permeate as a function of filtration time.

investigated wastewater is highly turbid, indicating the presence of a large amount of suspended matter [29]. It was discovered that 99.8% of wastewater turbidity was reduced, as shown in Fig. 20. Because rejected particles are larger than membrane pores, it is highly likely that the removal of turbidity by sand membrane occurred mostly by a sieving mechanism. As a result, it is reasonable to conclude that the sand MF membrane is effective in removing turbidity from citrus cleansing wastewater. In the case of COD, the rejection rate could be as high as 64%. (Fig. 20). The difference between rejected COD and residual COD in permeate is that rejected COD identifies solid particles (suspended and colloidal), whereas residual COD in permeate distinguishes soluble matters found below 240 mg/L [30]. As a result, the effectiveness of a sand membrane in reducing COD in citrus cleaning effluent has been demonstrated. conductivity rejection is not considerable, as expected, because soluble salts cannot be prevented by the membrane because the ions are too small to be rejected by the MF [31]. As a result, some asymmetry on the sand membrane is required to create UF or NF membranes that are likely to be suitable for the removal of soluble salt [29]. It should be noted that filtration time improves turbidity and COD rejections only little. The observed improvement is mostly due to the accumulation of rejected particles on the membrane surface, which forms a cake layer that acts as a secondary selective layer. This phenomenon is well-addressed in MF process [32].

4. Conclusion

The support membrane was successfully prepared and characterized using locally available sand materials. The paste composition and sintering conditions were chosen to favor an increase in mechanical resistance while maintaining a large porous volume and good chemical resistance to acid and basic solutions. Moreover, the active microfiltration layer created by the slip casting process has an excellent adherence to the support and a water permeability of 1,771.4 L/h/m^2 bar. Filtration effects confirmed that the membrane efficaciously eliminates all turbidity from citrus wash effluent beside of removal of 64% of COD. Therefore, sand membrane might be in all likelihood appropriate for remedy of different industrial wastewater.

References

[1] A. Agarwalla, K. Mohanty, Comprehensive characterization, development, and application of natural/Assam Kaolin-based ceramic microfiltration membrane, Mater. Today Chem., 23 (2022) 100649, doi: 10.1016/j.mtchem.2021.100649.
[2] N. El Qacimi, N. El Baraka, N. Saffaj, R. Mamouni, A. Laknifli, S. Alami Younssi, A. Faouzi, H. Zidouh, Preparation and characterization of flat membrane support based on Sahara Moroccan clay: application to the filtration of textile effluents, Desal. Water Treat., 143 (2019) 111–117.
[3] A. Belgada, B. Achiou, S. Alami Younssi, F.Z. Charik, M. Ouammou, J.A. Cody, R. Benhida, K. Khaless, Low-cost ceramic microfiltration membrane made from natural phosphate for pretreatment of raw seawater for desalination, J. Eur. Ceram. Soc., 41 (2021) 1613–1621.
[4] J. Usman, M.H. Dzarfan Othman, A. Fauzi Ismail, M.A. Rahman, J. Jaafar, Y. Olabode Raji, A.O. Gbadamosi, T.H. El Badawy, K.A. Mohamad Said Number, An overview of superhydrophobic ceramic membrane surface modification for oil-water separation, J. Mater. Res. Technol., 12 (2021) 643–667.
[5] M.B. Asif, Z. Zhang, Ceramic membrane technology for water and wastewater treatment: a critical review of performance, full-scale applications, membrane fouling and prospects, Chem. Eng. J., 418 (2021) 129481, doi: 10.1016/j.cej.2021.129481.
[6] H. Fang, J.F. Gao, H.T. Wang, C.S. Chen, Hydrophobic porous alumina hollow fiber for water desalination via membrane distillation process, J. Membr. Sci., 403–404 (2012) 41–46.
[7] S.L. Sandhya Rani, R.V. Kumar, Insights on applications of low-cost ceramic membranes in wastewater treatment: a mini-review, Case Stud. Chem. Environ. Eng., 4 (2021) 100149, doi: 10.1016/j.cscee.2021.100149.
[8] S. Bouzid Rekik, J. Bouaziz, A. Deratani, S. Baklouti, Study of ceramic membrane from naturally occurring-kaolin clays for microfiltration applications, Period. Polytech. Chem. Eng., 61 (2017) 206–215.
[9] A. Abdullayev, M.F. Bekheet, D.A.H. Hanaor, A. Gurlo, Materials and applications for low-cost ceramic membranes, Membranes (Basel), 9 (2019), doi: 10.3390/membranes9090105.
[10] N. Malik, V.K. Bulasara, S. Basu, Preparation of novel porous ceramic microfiltration membranes from fly ash, kaolin and dolomite mixtures, Ceram. Int., 46 (2020) 6889–6898.
[11] B. Achiou, H. Elomari, M. Ouammou, A. Albizane, J. Bennazha, S. Alami Younssi, A. Aaddane, Study of added starch on characteristics of flat ceramic microfiltration membrane made from natural Moroccan pozzolan, J. Mater. Environ. Sci., 9 (2018) 1–12, doi: 10.26872/jmes.2017.9.3.113.
[12] B. Achiou, H. Elomari, A. Bouazizi, A. Karim, M. Ouammou, A. Albizane, J. Bennazha, S. Alami Younssi, I.E. El Amrani, Manufacturing of tubular ceramic microfiltration membrane based on natural pozzolan for pretreatment of seawater desalination, Desalination, 419 (2017) 181–187.
[13] C. Sadik, A. Manni, S. El Kalakhi, I.E.E.A. El Hassani, Preparation and characterization of possible basic ceramics from Moroccan magnesite, J. Aust. Ceram. Soc., 55 (2019) 415–423.
[14] A. Manni, B. Achiou, A. Karim, A. Harrati, C. Sadik, M. Ouammou, S. Alami Younssi, A. El Bouari, New low-cost ceramic microfiltration membrane made from natural magnesite for industrial wastewater treatment, J. Environ. Chem. Eng., 8 (2020) 103906, doi: 10.1016/j.jece.2020.103906.
[15] N. El Baraka, A. Laknifli, N. Saffaj, M. Addich, A. Ait Taleb, A. Fatni, M. Ait Baih, Study of coupling photocatalysis and membrane separation using tubular ceramic membrane made from natural Moroccan clay and phosphate, E3S Web Conf., 150 (2020), doi: 10.1051/e3sconf/202015001007.

[16] S. Saja, A. Bouazizi, B. Achiou, M. Ouammou, A. Albizane, J. Bennazha, S. Alami Younssi, Elaboration and characterization of low-cost ceramic membrane made from natural Moroccan perlite for treatment of industrial wastewater, J. Environ. Chem. Eng., 6 (2018) 451–458.
[17] Y. Azougarh, M. Abbaz, N. Hafid, M. Benafqir, M. Ez-zahery, N. El Alem, Characterization and treatment of leachate of the great agadir discharge by infiltration–percolation onto titaniferous sand, Sci. Afr., 6 (2019), doi: 10.1016/j.sciaf.2019.e00154.
[18] S.A. Alftessi, M.H. Dzarfan Othman, M.R. Adam, T.M.Farag, A.F. Ismail, M.A. Rahman, J. Jaafar, A. Habib, Y.O. Raji, S.K. Hubadillah, Novel silica sand hollow fibre ceramic membrane for oily wastewater treatment, J. Environ. Chem. Eng., 9 (2021) 104975, doi: 10.1016/j.jece.2020.104975.
[19] A. Tahiri, L. Messaoudi, N. Tijani, M.H. Zerrouk, M. Messaoudi, Manufacture and characterization of flat membrane supports based on Moroccan Rif clay, Mater. Today:. Proc., 43 (2020) 209–215, doi: 10.1016/j.matpr.2020.11.638.
[20] S. Saja, A. Bouazizi, B. Achiou, H. Ouaddari, A. Karim, M. Ouammou, A. Aaddane, J. Bennazha, S. Alami Younssi, Fabrication of low-cost ceramic ultrafiltration membrane made from bentonite clay and its application for soluble dyes removal, J. Eur. Ceram. Soc., 40 (2020) 2453–2462.
[21] L.N.F. Queiroga, M.B.B. Pereira, L.S. Silva, E.C. Silva Filho, I.M.G. Santos, M.G. Fonsecaa, T. Georgelin, M. Jaber, Microwave bentonite silylation for dye removal: influence of the solvent, Appl. Clay Sci., 168 (2018) 478–487.
[22] H. Ouaddari, A. Karim, B. Achiou, S. Saja, A. Aaddane, J. Bennazha, I. El Amrani El Hassani, M. Ouammou, A. Albizane, New low-cost ultrafiltration membrane made from purified natural clays for direct Red 80 dye removal, J. Environ. Chem. Eng., 7 (2019) 103268, doi: 10.1016/j.jece.2019.103268.
[23] A.S. Khan, H. Khalid, Z. Sarfraz, M. Khan, J. Iqbal, N. Muhammed, A. Fareed, Vibrational spectroscopy of selective dental restorative materials, Appl. Spectrosc. Rev., 52 (2017) 507–540.
[24] C.A. Yanu, J.M. Sieliechi, M.B. Ngassoum, Optimization of ceramic paste viscosity use for the elaboration of tubular membrane support by extrusion and its application, J. Mater. Sci. Chem. Eng., 8 (2020) 1–22, doi: 10.4236/msce.2020.83001.
[25] M. Ait Baih, H. Saffaj, K. Aziz, A. Bakka, N. El baraka, H. Zidouh, R. Mamouni, N. Saffaj, Statistical optimization of the elaboration of ceramic membrane support using Plackett-Burman and response surface methodology, Mater. Today:. Proc., 52 (2022) 128–136.
[26] N. El Baraka, N.Saffaj, R. Mamouni, M. El Haddad, A. Laknifli, S. Alami Younssi, M. Aboulkacem, A. Roudani, New bio ceramic support membrane from animal bone, J. Microbiol. Biotechnol. Res., 3 (2013) 1–6.
[27] A. Ait Taleb, N. El Baraka, N. Saffaj, A. Laknifli, R. Mamouni, A. Fatni, A. El Hammadi, N. El Qacimi, New Tubular ceramic membranes from natural Moroccan clay for microfiltration application, E3S Web Conf., 37 (2018) 53–60.
[28] H. Aloulou, H. Bouhamed, R. Ben Amar, S. Khemakhem, New ceramic microfiltration membrane from tunisian natural sand: application for tangential wastewater treatment, Desal. Water Treat., 78 (2017) 41–48.
[29] A. Fatni, A. El Hammadi, R. Bouaddi, A.A. Taleb, N. El Baraka, A. Laknifli, Experimental design applied to improve the efficiency and the performance of the reverse osmosis process, Desal. Water Treat., 236 (2021) 45–54.
[30] Y. Zheng, S. Yu, S. Shuai, Q. Zhou, Q. Cheng, M. Liu, C. Gao, Color removal and COD reduction of biologically treated textile effluent through submerged filtration using hollow fiber nanofiltration membrane, Desalination, 314 (2013) 89–95.
[31] F. Labarca, R. Bórquez, Comparative study of nanofiltration and ion exchange for nitrate reduction in the presence of chloride and iron in groundwater, Sci. Total Environ., 723 (2020) 137809, doi: 10.1016/j.scitotenv.2020.137809.
[32] B. Alaei, R. Amiri Chayjan, M. Ali Zolfigol, Tomato juice microfiltration process assisted with pressure-vacuum combination condition: a physico-chemical investigation and optimization, Biosyst. Eng., 212 (2021) 62–76.